Are Heterogeneous Graph Neural Networks Truly Effective? A Causal Perspective

Xiao Yang^a, Xuejiao Zhao^{b,c}, Zhiqi Shen^a

a organization=College of Computing and Data Science, Nanyang Technological
 University, country=Singapore
 b organization=Joint NTU-UBC Research Centre of Excellence in Active Living for the
 Elderly (LILY), Nanyang Technological University, country=Singapore
 c organization=Alibaba-NTU Singapore Joint Research Institute (ANGEL), Nanyang
 Technological University, country=Singapore

Abstract

Graph neural networks (GNNs) have achieved remarkable success in node classification. Building on this progress, heterogeneous graph neural networks (HGNNs) integrate relation types and node and edge semantics to leverage heterogeneous information. Causal analysis for HGNNs is advancing rapidly, aiming to separate genuine causal effects from spurious correlations. However, whether HGNNs are intrinsically effective remains underexamined, and most studies implicitly assume rather than establish this effectiveness. In this work, we examine HGNNs from two perspectives: model architecture and heterogeneous information. We conduct a systematic reproduction across 21 datasets and 20 baselines, complemented by comprehensive hyperparameter retuning. To further disentangle the source of performance gains, we develop a causal effect estimation framework that constructs and evaluates candidate factors under standard assumptions through factual and counterfactual analyses, with robustness validated via minimal sufficient adjustment sets, cross-method consistency checks, and sensitivity analyses. Our results lead to two conclusions. First, model architecture and complexity have no causal effect on performance. Second, heterogeneous information exerts a positive causal effect by increasing homophily and local-global distribution discrepancy, which makes node classes more distinguishable. The implementation is publicly available at https://github.com/YXNTU/CausalHGNN.

Keywords: Heterogeneous Graph Neural Networks, Node Classification, Causal-Effect

1. Introduction

Node classification is a cornerstone task in graph learning [1, 2, 3, 4], with broad applications in various domains [5, 6, 7], such as recommendation systems [8, 9, 10], risk detection [11, 12], bioinformatics [13, 14, 15] and drug development [16, 17]. Graph neural networks (GNNs) [18, 19, 20] have emerged as a powerful framework by leveraging graph topology and node features through message passing [21, 22]. However, traditional GNNs are primarily designed for homogeneous graphs, limiting their ability to model the diverse semantics in real-world networks [23, 24]. To capture such heterogeneity, heterogeneous graph neural networks (HGNNs) [25, 26] extend GNNs by incorporating heterogeneous information to represent multiple node and edge types.

From a causal perspective, analyzing learning problems has become increasingly mainstream [27, 28, 29]. Recent studies have introduced causal perspectives into heterogeneous graph learning to disentangle genuine causal contributions from spurious correlations [30, 31]. For instance, Adhikari et al. [32] applied causal analysis to balance heterogeneous peer influence, Zhao et al. [33] proposed Dual Weighting Regression to capture neighbor interference and mitigate network bias, and Wu et al. [34] estimated heterogeneous causal effects to enhance HGNN adaptability to downstream tasks. These efforts demonstrate that causal analysis can provide valuable insights into the mechanisms of HGNNs. However, all existing approaches implicitly assume that HGNNs are inherently effective rather than verifying this assumption. If this premise does not hold, causal conclusions built upon it may be unreliable. Prior empirical evidence [35], in contrast, shows that HGNNs do not consistently outperform simpler GNNs on heterogeneous graph benchmarks. This tension leads to a fundamental question: are HGNNs genuinely effective, and if so, what underlying factors drive their performance and how can these contributions be rigorously assessed?

To answer this question, we first clarify the role of model architecture in HGNNs. We reproduce 20 widely used baselines across 21 heterogeneous graph datasets using their official implementations under a unified evaluation protocol, ensuring that comparisons are not confounded by inconsistent training procedures. In parallel, we perform extensive hyperparameter tuning for a representative and simple HGNN, RGCN [36], and compare its optimized results with all reproduced baselines. With model-related effects controlled, we next focus on performance variations arising from heterogeneous infor-

mation itself. We consider two graph characteristics that have been formally recognized as critical to representation learning: homophily [37, 38, 39, 40] and local—global distribution discrepancy [41, 42, 43]. Based on these two factors, we construct candidate measures that capture their influence, retain those meeting statistical significance and effect-size criteria, and evaluate them through causal inference analyses. Specifically, we perform factual and counterfactual evaluations at both group and individual levels, and verify robustness through minimal adjustment sets, cross-method consistency, and sensitivity analyses.

Our empirical results lead to two main conclusions. First, model architecture and complexity have no causal influence on performance. After comprehensive hyperparameter tuning, RGCN [36] achieves better results than other HGNN baselines, indicating that the advantage is not attributable to architectural design itself. Second, causal effect analysis shows that heterogeneous information plays a decisive role. Collapsing the graph into a homogeneous projection leads to a marked drop in accuracy. This decline arises because the removal of heterogeneous information weakens key structural signals by reducing homophily and diminishing the local–global distribution discrepancy, which lowers the separability of node classes and consequently increases misclassification. Together, these findings establish that the causal advantage of HGNNs originates from the structural information carried by heterogeneity rather than from model complexity.

In summary, our main contributions are as follows:

- We present the most comprehensive benchmark to date for heterogeneous graph learning, covering 20 HGNN baselines across 21 datasets under a unified evaluation protocol.
- We establish that model architecture and complexity have no causal effect on node classification performance, showing that performance gains cannot be attributed to architectural design.
- We identify that heterogeneous information has a positive causal effect on performance by strengthening structural signals, particularly homophily and the difference between local and global label distributions.

2. Related Work

2.1. HGNNs

Node classification is the primary task driving the development of HGNNs, and most existing work has focused on designing models that can effectively leverage heterogeneous information. These models can be roughly divided into three categories. The first category treats heterogeneous graphs as relational graphs, directly modeling information within each semantic. Representative methods include RGCN [36], which applies relation-specific transformations on adjacency matrices, HetGNN [25], which samples neighbors across node types, and HGT [44], which incorporates type-specific parameters into a heterogeneous attention mechanism. The second category relies on meta-paths to capture semantic dependencies. HAN [45] pioneered this approach by attending over manually defined meta-paths, MAGNN [46] further enriched semantic encoding with multiple meta-path encoders, and GTN [47] automated the construction of meta-paths via graph transformation layers. The third category moves beyond message passing and explores specialized architectures. For example, NSHE [48] samples heterogeneous subgraphs under multiple modes, while HINormer [49] and related Transformer-style models [50] introduce global attention and positional encodings to flexibly model heterogeneity.

2.2. Causal Effect Estimation on Graphs

Causal effect analysis originates from the Rubin Causal Model (RCM) [51, 52] and has been increasingly extended to graphs, where both structural dependencies and confounding pose unique challenges. Cotta et al. [53] introduced causal lifting for link prediction, leveraging invariances to answer counterfactual queries and explain how graph symmetries govern causal link formation. Chen et al. [54] proposed CIE, which applies backdoor adjustment to disentangle causal and spurious features, thereby explaining how data biases in graphs influence node classification. Sun et al. [55] further extended this direction to temporal knowledge graphs with CEGRL-TKGR, which disentangles causal and confounding representations via intervention to explain how event relationships drive link prediction. Beyond representation disentanglement, a growing body of work has focused on estimating treatment effects under network interference. Jiang et al. [56] estimated individual, peer, and total treatment effects from networked observational data, while Wu et al. [34] employed orthogonal causal learning to capture heterogeneous direct

and spillover effects. Du et al. [57] used causal mediation analysis to disentangle peer direct, peer indirect, and self-treatment effects, and Adhikari et al. [32] inferred direct individual causal effects under heterogeneous peer influence. Several methods explicitly address bias reduction in effect estimation: Farzam et al. [58] proposed geometric causal analysis with Ricci curvature to improve ITE estimation, Cai et al. [59] derived causal generalization bounds to explain how reweighting mitigates confounding bias, Hu et al. [60] developed disentangled causal analysis to separate adjustment from confounders, Sui et al. [61] introduced invariant graph learning to capture stable confounders and spillover effects, and Zhao et al. [33] proposed dual weighting regression to address heterogeneous network interference. Wang [62] proposed an LLM-guided divide-and-conquer framework for large-scale causal discovery. Beyond methodological advances, causal effect analysis has also been applied to domain-specific tasks: Ban [63] proposed an expert-free causal discovery method leveraging knowledge graph priors. Begum et al. [64] designed a Granger causality-inspired GNN to explain temporal dependencies in IoT traffic, Gao et al. [65] introduced diminutive causal structures and interchange interventions to improve GNN performance, Khaled et al. [66] extracted causal dependencies via transfer entropy for traffic prediction. Together, these works demonstrate that causal effect estimation on graphs not only advances methodological foundations for treatment effect estimation under interference, but also provides powerful explanatory tools across diverse graph-based applications.

3. Preliminaries

3.1. Potential Outcomes Framework (Rubin Causal Model)

The Rubin Causal Model (RCM) [51] formalizes causal effects using potential outcomes. Consider a population of units indexed by $i \in \{1, ..., n\}$. For each unit i, let $T_i \in \{0, 1\}$ denote a binary treatment indicator, where $T_i = 1$ indicates treatment and $T_i = 0$ indicates control. The potential outcomes are $Y_i(1)$ and $Y_i(0)$, representing the outcome of unit i under treatment and control, respectively. The observed outcome is then

$$Y_i = T_i Y_i(1) + (1 - T_i) Y_i(0). (1)$$

The fundamental problem of causal inference is that only one of the two potential outcomes can be observed for each unit. At the population level, let Y(1) and Y(0) denote the random variables representing the treatment and control potential outcomes across units. The average treatment effect (ATE) is defined as

$$ATE = \mathbb{E}[Y(1) - Y(0)], \tag{2}$$

where $\mathbb{E}[\cdot]$ denotes expectation over the population distribution.

To identify ATE from observational data, the following assumptions are commonly imposed:

- Stable Unit Treatment Value Assumption (SUTVA): no interference between units and a well-defined treatment for each unit.
- Ignorability: $(Y(1), Y(0)) \perp T \mid Z$, given observed covariates Z.¹
- Overlap: $0 < \Pr(T = 1 \mid Z) < 1$ for all Z in its support.

For binary outcomes $Y \in \{0,1\}$, the observed difference in event rates,

$$\Pr(Y = 1 \mid T = 1) - \Pr(Y = 1 \mid T = 0), \tag{3}$$

is referred to as the risk difference (also called lift in applied domains). In randomized experiments, this directly provides an unbiased estimator of the ATE, while in observational studies it is valid under ignorability and overlap.

3.2. Validity Criteria for Factual Analysis

We consider n independent observations indexed by i = 1, ..., n. Each observation has a binary treatment $T_i \in \{0, 1\}$, where $T_i = 1$ indicates treatment and $T_i = 0$ control, and a binary outcome $Y_i \in \{0, 1\}$, where $Y_i = 1$ indicates event occurrence and $Y_i = 0$ otherwise.

3.2.1. Sample adequacy

Valid inference requires sufficient sample size in both treatment and control groups, and adequate counts for both outcome categories [67]. Define group sizes

$$n_1 = \sum_{i=1}^{n} \mathbf{1}(T_i = 1), \quad n_0 = \sum_{i=1}^{n} \mathbf{1}(T_i = 0),$$
 (4)

 $^{^{1}\}bot$ denotes conditional independence.

where $\mathbf{1}(\cdot)$ is the indicator function. Define event rates

$$p_t = \frac{1}{n_t} \sum_{i:T_i = t} Y_i, \quad t \in \{0, 1\}.$$
 (5)

Adequacy requires

$$n_1 \ge n_{\min}, \quad n_0 \ge n_{\min}, \quad n_t p_t \ge s_{\min}, \quad n_t (1 - p_t) \ge s_{\min}, \quad t = 0, 1,$$
 (6)

where n_{\min} is the minimal group size and s_{\min} the minimal expected cell count.²

3.2.2. Statistical significance

The empirical ATE is

$$\hat{ATE} = p_1 - p_0, \tag{7}$$

with standard error

$$SE = \sqrt{\frac{p_1(1-p_1)}{n_1} + \frac{p_0(1-p_0)}{n_0}}.$$
 (8)

The z-statistic is

$$z = \frac{\hat{ATE}}{SE} \sim \mathcal{N}(0, 1), \tag{9}$$

under the large-sample normal approximation. We test

$$H_0: ATE = 0 \text{ vs. } H_1: ATE \neq 0,$$
 (10)

and reject H_0 if |z| exceeds the critical value at the chosen significance level [68].

3.2.3. Multiple testing correction

When m hypotheses are tested, we control the false discovery rate (FDR) using the Benjamini–Hochberg (BH) procedure [69]. Let ordered p-values be $p_{(1)} \leq \cdots \leq p_{(m)}$. For target FDR $\alpha \in (0,1)$, reject

$$H_{(1)}, \dots, H_{(k^*)}, \quad k^* = \max \left\{ i : p_{(i)} \le \frac{i}{m} \alpha \right\}.$$
 (11)

The BH-adjusted p-values (q-values) are computed as

$$q_{(i)} = \min_{j>i} \left(\frac{m}{j} \, p_{(j)}\right) \wedge 1,\tag{12}$$

²A common rule of thumb for 2×2 tables is $s_{\min} \geq 5$ [67].

via backward recursion:

$$q_{(m)} = p_{(m)},$$
 (13)

$$q_{(i)} = \min\left\{\frac{m}{i} p_{(i)}, q_{(i+1)}\right\}, \quad i = m - 1, \dots, 1.$$
 (14)

A result is significant if $q \leq \alpha$. Under independence or PRDS (positive regression dependence on a subset), BH guarantees FDR $\leq \alpha$.

3.2.4. Practical Significance

Statistical significance does not necessarily imply practical importance [70]. To quantify the magnitude of observed effects, we report both the absolute and relative changes in outcome probabilities:

$$RD = p_1 - p_0, RE = \frac{p_1}{p_0}, (15)$$

where $p_1 = P(Y=1 \mid T=1)$ and $p_0 = P(Y=1 \mid T=0)$. Here RD (risk difference, also called lift) measures the absolute improvement, while RE (relative effect ratio) measures the relative improvement between treated and control groups. Thresholds for practical relevance depend on the application domain (for example, clinical or policy standards). This analysis complements statistical significance testing by clarifying whether the estimated causal effects are large enough to be meaningful in practice.

4. Establishing and Explaining the Effectiveness of HGNNs

Figure 1 illustrates our three-step causal audit of heterogeneous graph neural networks (HGNNs). Step 1 examines whether performance gains arise from architectural sophistication. Step 2 tests whether heterogeneous graphs themselves contribute beyond model design. Step 3 investigates which structural factors of heterogeneity explain the observed benefits.

4.1. Step 1: Is performance driven by model architecture?

Existing studies often take the effectiveness of heterogeneous information for granted and instead focus on designing increasingly sophisticated HGNN architectures. This practice risks conflating two potential sources of performance gains: the use of heterogeneous information and the complexity of model design. To ensure a valid causal effect estimation, it is necessary to first rule out model architecture as a confounding factor.

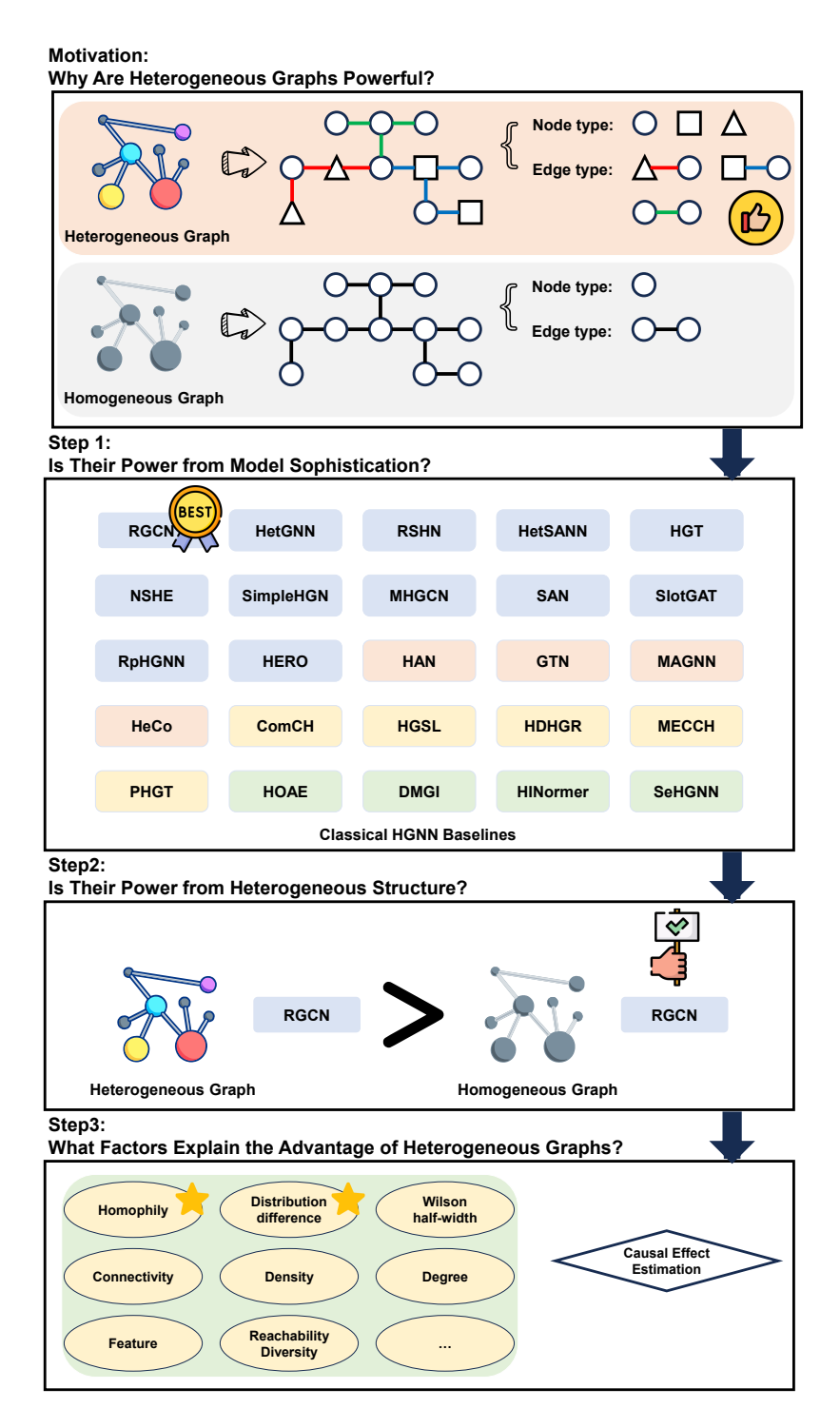


Figure 1: Overview of our research roadmap for disentangling the causal effects of heterogeneous information. \$9\$

We therefore reproduce 20 representative HGNN baselines, summarized in Table 1, and apply them across 21 heterogeneous graph datasets from nine sources. These baselines cover four categories: relation-based, meta-path-based, hybrid (relation & meta-path), and non-message-passing models. All implementations strictly follow the official repositories with their reported hyperparameters, while cases containing implementation errors are replaced by the corresponding OpenHGNN implementations [71].

In addition, motivated by findings in homogeneous graphs where the simplest model (GCN [72]) can match or even outperform more complex designs [73], we comprehensively retune the simplest heterogeneous model, RGCN [36], across all datasets. This unified reproduction and hyperparameter retuning enable a fair comparison between RGCN and more sophisticated HGNNs, isolating the causal effect of model architecture from that of heterogeneous information.

Type	Model
	HetGNN [25], RSHN [74], SimpleHGN [35], MHGCN [75]
Relation	SlotGAT [76], RpHGNN [77], HERO [78], SAN [79]
	HetSANN [80], HGT [44], NSHE [48]
Meta-path	HAN [45], GTN [47], MAGNN [46], HeCo [81]
Relation & meta-path	ComCH [82], HGSL [83], HDHGR [84]
neration & meta-path	MECCH [85], PHGT [86]
No message-passing	HOAE [87], DMGI [88], HINormer [49], SeHGNN [50]

Table 1: Reproduction of HGNN baselines. All models are reproduced strictly following their official implementations with paper-reported hyperparameters. For Relation models, OpenHGNN [71] is used when the official repository contains implementation errors.

The results in Table 2 reveal three main findings. First, the performance of RGCN has been consistently underestimated. With systematic hyperparameter tuning, RGCN achieves substantial improvements across datasets. For example, on AIFB the reported accuracy is 91.67, while our tuned RGCN reaches 100 (+8.33); on MUTAG, the reported score is 72.06, compared to 84.58 (+12.52) after tuning. These examples illustrate that tuning yields consistent gains beyond previously reported numbers. Second, apart from a few marginal cases, the fine-tuned RGCN outperforms the majority of HGNN models. For instance, on DBLP the Macro F1 and Micro F1 of SlotGAT (94.86 and 95.27) are slightly higher than those of RGCN (94.65 and 95.00). Beyond such small differences, RGCN clearly surpasses most baselines: on DBLP it improves upon HGT by more than six points in both metrics, and

	Hete	GNN	RS	SHN	SAN	HetS	SANN		GTN	
Source	Acac	lemic	AIFB	MUTAG	Alibaba	IM		ACM	IMDB	DBLP
Metric	MaF1	MiF1	Acc	Acc	MaF1	MaF1	MiF1	MaF1	MaF1	MaF1
model*	97.80	97.90	97.22	82.35	45.14	73.86	72.00	92.68	60.92	94.18
RGCN*	-	-	91.67	72.06	22.71	67.13	62.58	-	-	-
model	97.80	97.90	97.22	82.35	45.10	72.51▼	70.06▼	92.21	57.37▼	92.93▼
RGCN	98.47	98.48	100▲	$84.58 \blacktriangle$	$56.30 \blacktriangle$		$71.14 \blacktriangle$	92.63	59.69	93.87
	NS	HE		Simple	eHGN		MH	GCN		GNN
Source	A(CM	A	CM	DE	BLP	DE	BLP	A	CM
Metric	MaF1	MiF1	MaF1	MiF1		MiF1	MaF1	MiF1	MaF1	MiF1
model*	83.27	84.12	93.42	93.35	94.01	94.46	94.50	95.20	94.09	94.04
RGCN*	-	-	91.55	91.41	91.52	92.07	-	-	91.55	91.41
model	84.78▲	84.95▲	93.23	93.15	93.75	94.18	93.17▼	93.75▼	93.44	93.37
RGCN	93.21	93.10	$94.11 \blacktriangle$	$94.02 \blacktriangle$	$94.65 \blacktriangle$	$95.00 \blacktriangle$		93.75		$94.02 \blacktriangle$
				ERO			H.	AN	MA	GNN
Source	A(CM	Y	elp	DE	BLP	A	CM	DE	BLP
Metric	MaF1	MiF1	MaF1	MiF1	MaF1	MiF1		MiF1		MiF1
model*	92.20	92.10	92.40	92.30	93.80	94.40	91.89	91.85	93.13	93.61
RGCN*	-	-		-	-		-	-		
model	91.52	91.44	92.58▲	92.20	93.11		90.63▼	90.61▼	92.81	93.36
RGCN	92.55	92.46	93.25	92.84	93.94	94.71	92.45	92.50	93.06	93.59
				GSL				PH		
Source			Y	elp	DE	BLP	A	CM	DE	
Metric	MaF1	MiF1			MaF1		MaF1			MiF1
model*	93.48	93.37	93.55	92.76	91.92	92.77	93.79	93.72	94.96	95.33
RGCN*	-	-	-	-	-	-	91.55	91.41	91.52	92.07
model	92.95	92.84	92.83	92.20	91.68	92.53	84.78▼		93.83▼	
RGCN	92.63	92.54	93.25	92.84	91.16	92.06	94.11▲	$94.02 \blacktriangle$		95.00▲
		AE			DMGI					ormer
Source	AC			CM				azon		
Metric	MaF1	MiF1	MaF1	MiF1	MaF1		MaF1	MiF1	MaF1	MiF1
model*	93.11	93.03	89.80	89.80	64.80		74.60	74.80	94.57	94.94
RGCN*	-	-	-		-	-	-	=	91.52	92.07
model	93.10	93.05	84.72▼		61.18▼	61.64▼	73.42	74.01	94.02	94.45
RGCN	93.21	93.10	89.49	89.39	63.48	63.95	73.76	74.45	94.65▲	95.00▲
	T) (F	IGT	BLP		Slot			HDI	HGR
Source	IM M-E1			3LP		JM M:D1		BLP	IM M-E1	
Metric	MaF1	MiF1	MaF1		MaF1	MiF1	MaF1	MiF1	MaF1	MiF1
model*	49.18	49.37	86.46	87.23	93.99		94.95	95.31	58.97	
RGCN*	- 40.01	40.51	- 00.40	- 07.00	91.55	91.41	91.52	92.07	50.33	52.51
$_{ m model}$	49.21 58.97	49.51	86.40	87.28	93.95	94.00	94.86	95.27 95.00▲	- 50.07 A	- FO F1 A
NGCN		59.51 CCH		93.59		94.02	94.65▲	95.00 SeH	58.97▲	59.51▲
Correct	DE	OLD.	116 A	eCo CM	COI	BLP	Λ.	Sen	DE	DI D
Source	MaF1	MiF1	MaF1		MaF1		MaF1	MiF1		MiF1
Metric model*	94.34	95.08	89.04	88.71	94.29	94.70	94.05	93.98	95.06	95.42
RGCN*	94.34	93.41	89.04	88.71	94.29	94.70	94.05 91.55		95.06	95.42
model	93.99	93.41	88.66	88.35	93.66	93.91	93.82	91.41 93.74	91.52	92.07 95.26
model RGCN	93.99	94.75 94.66▲	93.21	88.33 93.10	93.00 94.35	93.91 94.87	93.82 94.11 ▲	93.74 94.02 ▲	94.90 94.65▲	95.26 95.00▲
110011	<i>99.</i> 01 ▲	∂4.00 ▲	99.41	99.10	94.00	94.01	94.11	J4.U4	∂4.UU▲	39.00 <u> </u>

Table 2: Reproduction results of 20 HGNN baselines on 21 datasets. For each model, model* and RGCN* denote the results reported in the original papers, model denotes our reproduction using the official implementation and reported hyperparameters, and RGCN denotes our hyperparameter tuned results. **Abbreviations:** $MaF1 = Macro\ F1,\ MiF1 = Micro\ F1,\ Acc = Accuracy.$

ACM-A				RGCN
AUM-A	HAN,DMGI	Macro F1	85.46	89.49
	•	Micro F1	85.74	89.39
ACM-B	HGT,GTN,HGSL,MECCH	Macro F1	83.58	92.63
ACM-C	NSHE,HeCo,HOAE	Macro F1	82.30	93.21
ACM ACMI-C	TVSIIL,IICCO,IICTL	Micro F1	82.44	93.10
ACM-D	HERO	Macro F1	89.92	92.55
NOM-D		Micro F1	89.94	92.46
ACM-E	${\bf SlotGAT,} {\bf RpHGNN,} {\bf PHGT}$	Macro F1	91.96	94.11
	HDHGR,SimpleHGN,SeHGNN	Micro F1	91.88	94.02
IMDB-A	HAN,DMGI	Macro F1	61.84	63.48
	,	Micro F1	62.72	63.95
IMDB IMDB-B	GTN,MECCH	Macro F1	49.38	59.69
IMDB-C	HetSANN,HGT,MAGNN	Macro F1	66.97	73.71
	•	Micro F1	58.33	71.14
DBLP-A	GTN,MECCH	Macro F1	85.88	93.87
DBLP-B	HGSL	Macro F1	85.82	91.16
DDLI -D		Micro F1	86.81	92.06
DBLP-C	${\it HetSANN, HGT, MAGNN, HeCo}$	Macro F1	87.85	93.06
DDLI -C		Micro F1	88.81	93.59
DBLP-D	MHGCN	Macro F1	88.99	93.18
DBLP DBLI -D	WIIIGON	Micro F1	90.10	93.75
DBLP-E	HERO,HAN	Macro F1	88.52	93.94
DDLI -E	,	Micro F1	89.61	94.71
DBLP-F	Simple HGN, Slot GAT, RpHGNN	Macro F1	87.00	94.65
DDLI -I	HDHGR,HINormer,SeHGNN,PHGT	Micro F1	88.33	95.00
DBLP-G	ComCH	Macro F1	92.26	94.35
DDLI -Q		Micro F1	92.31	94.87
Academic MC	HetGNN	Macro F1	97.75	98.47
Academic MC	HeiGININ	Micro F1	97.79	98.48
Yelp Yelp	HERO,HGSL	Macro F1	88.52	93.94
reip reip	HERO,HGSL	Micro F1	89.61	94.71
Alibaba Event	SAN	Macro F1	42.32	56.30
AIFB AIFB	RGCN,RSHN	Accuracy	97.22	100.00
MUTAG MUTAG	RGCN,RSHN	Accuracy	79.41	84.58
Amazon Amazon-A	DMGI	Macro F1	68.02	73.76
Amazon Amazon-A	DMGI	Micro F1	69.16	74.45

Table 3: Comparison between GCN on homogeneous graphs and RGCN on heterogeneous graphs across 21 datasets. Results are reported in terms of Macro F1, Micro F1, or Accuracy depending on dataset convention.

on ACM it achieves around nine points higher than PHGT. These results show that once properly tuned, RGCN not only matches but often exceeds more sophisticated HGNN architectures. Third, some HGNN models show a clear performance drop when reproduced, yet the tuned RGCN still surpasses even their originally reported results. For example, on ACM the reproduced PHGT achieves only 84.78 Macro F1 and 85.62 Micro F1, far below its reported 93.79 and 93.72. Nevertheless, our tuned RGCN attains 94.11 Macro F1 and 94.02 Micro F1, higher than the original PHGT numbers, reinforcing that model architecture is not the decisive factor.

In summary, the superior performance observed on heterogeneous graphs cannot be attributed to architectural complexity. After rigorous hyperparameter optimization, RGCN as the simplest HGNN architecture consistently outperforms most competing models and in many cases even surpasses the published results of advanced HGNNs. This motivates us to shift focus from model design to the causal contribution of heterogeneous information itself.

4.2. Step 2: Do heterogeneous graphs help beyond architecture?

Having established in Step 1 that model architecture is not the primary source of performance gains, we now turn to the role of heterogeneous information itself. Our experimental design is grounded in the following rationale. On homogeneous graphs, GCN has been shown to be a simple yet highly competitive baseline and is widely regarded as a representative architecture [72]. Analogously, Step 1 demonstrated that, after systematic hyperparameter optimization, RGCN serves as a strong representative for HGNNs. To disentangle the contribution of heterogeneity, it is therefore appropriate to compare these two canonical models under matched conditions: RGCN operating on heterogeneous graphs and GCN operating on their homogeneous projections. Such a comparison ensures that any performance differences can be attributed to heterogeneous information, rather than to architectural design.

Concretely, for each of the 21 heterogeneous graph datasets, we construct its homogeneous counterpart by removing all node and edge type information and then train GCN with its best-tuned hyperparameters on the resulting graph. In parallel, RGCN is trained on the original heterogeneous graph with its own optimized hyperparameters, thereby evaluating both models under their respective optimal configurations. The results, summarized in Table 3, show that RGCN consistently outperforms GCN across datasets and

evaluation metrics, often with substantial margins. For instance, on IMDB-C the Macro F1 improves from 66.97 with GCN to **73.71** with RGCN, and on AIFB the accuracy rises from 97.22 with GCN to **100.00** with RGCN. Similar gains are observed on larger-scale benchmarks such as ACM and DBLP, where RGCN achieves 5–10 points higher in both Macro F1 and Micro F1. These findings provide strong evidence that the effectiveness of HGNNs originates from heterogeneous information, thereby establishing a positive causal effect attributable to heterogeneity itself.

4.3. Step 3: What factors make heterogeneity useful?

The analyses in Steps 1 and 2 have established that architectural complexity is not the decisive factor and that heterogeneous information exerts a positive causal effect on node classification. The key question that follows is why heterogeneity improves performance. In particular, it remains unclear which structural properties are enhanced by heterogeneous information and how these properties make node classes more distinguishable. To address this question, we design a causal validation framework that combines factual analysis, counterfactual analysis, and complementary validation. This framework quantifies node-level treatment effects and systematically evaluates candidate structural metrics, enabling us to identify the mechanisms through which heterogeneous information strengthens class-relevant signals.

4.3.1. Identifying Possible Factors

To explain why heterogeneous information benefits node classification, we focus on two structural factors that have been shown to be critical: homophily and local-global distribution discrepancy. Let $\mathcal{G} = (\mathcal{V}, \mathcal{E}, \mathcal{R})$ be a heterogeneous graph with node set \mathcal{V} , edge set \mathcal{E} , and relation set \mathcal{R} . For comparison, let $G = (\mathcal{V}, \mathcal{E}')$ denote its homogeneous projection obtained by discarding node and edge types. Given a node $v \in \mathcal{V}$ and a relation $r \in \mathcal{R}$, denote by $\mathcal{N}_r(v)$ the neighborhood of v under relation r, with size $n_r(v) = |\mathcal{N}_r(v)|$. The two factors are defined as follows.

Homophily.. Homophily measures the label agreement between a node and its neighbors.³

$$H_r(v) = \frac{1}{n_r(v)} \sum_{u \in \mathcal{N}_r(v)} \mathbf{1}[y(u) = y(v)].$$
 (16)

Local-global distribution discrepancy.. This factor measures how different the local label distribution is from the global distribution.

$$p_r(c \mid v) = \frac{1}{n_r(v)} \sum_{u \in \mathcal{N}_r(v)} \mathbf{1}[y(u) = c], \quad p_{\text{glob}}(c) = \frac{1}{|\mathcal{V}|} \sum_{u \in \mathcal{V}} \mathbf{1}[y(u) = c].$$
 (17)

The total variation distance is

$$D_r(v) = \frac{1}{2} \sum_{c=1}^{C} |p_r(c \mid v) - p_{\text{glob}}(c)|.$$
 (18)

Relation-level aggregation.. Since each heterogeneous graph may contain multiple relations, we aggregate metrics across all $r \in \mathcal{R}$. For either $M \in \{H, D\}$, we compute

$$M_{\min}(v) = \min_{r \in \mathcal{R}} M_r(v), \quad M_{\max}(v) = \max_{r \in \mathcal{R}} M_r(v), \quad M_{\text{avg}}(v) = \frac{1}{|\mathcal{R}|} \sum_{r \in \mathcal{R}} M_r(v).$$
(19)

4.3.2. Experimental Setup

We first evaluate whether heterogeneous information benefits each node in terms of predictive accuracy. Given a heterogeneous graph $\mathcal{G} = (\mathcal{V}, \mathcal{E}, \mathcal{R})$ and its homogeneous projection $G = (\mathcal{V}, \mathcal{E}')$, we train RGCN on \mathcal{G} and GCN on G, each repeated s independent runs⁴ with different random seeds. For every node $v \in \mathcal{V}$, we record the empirical success probabilities

$$\hat{\pi}_{\mathcal{G}}(v) = \frac{1}{s} \sum_{t=1}^{s} \mathbf{1} [\hat{y}_{\mathcal{G}}^{(t)}(v) = y(v)], \qquad \hat{\pi}_{G}(v) = \frac{1}{s} \sum_{t=1}^{s} \mathbf{1} [\hat{y}_{G}^{(t)}(v) = y(v)]. \quad (20)$$

We then define a treatment indicator

$$T(v) = \mathbf{1}[\hat{\pi}_{\mathcal{G}}(v) > \hat{\pi}_{G}(v)], \qquad (21)$$

³In this paper, homophily is computed as the proportion of neighbors whose labels match the central node, following [89].

 $^{^4}s = 5$ in this paper.

which equals 1 if node v achieves higher predictive accuracy under heterogeneous information.

Next, we quantify how the structural factors change when heterogeneity is removed. For each node v, we compute $H_r(v)$ and $D_r(v)$ on \mathcal{G} for every relation $r \in \mathcal{R}$, and aggregate them into

$$M_{\min}(v), \ M_{\max}(v), \ M_{\text{avg}}(v), \ M \in \{H, D\}.$$
 (22)

On the homogeneous projection G, only a single value $M^G(v)$ exists for each factor M. We therefore define binary comparison indicators

$$Z_{M,A}(v) = \mathbf{1} \left[M^G(v) < M_A^{\mathcal{G}}(v) \right], \qquad A \in \{\min, \max, \arg\}.$$
 (23)

For instance, if $H_{\min}(v) < H^G(v)$, $H_{\max}(v) < H^G(v)$, and $H_{\text{avg}}(v) > H^G(v)$, then the corresponding indicators are (0,0,1).

Together, the treatment variable T(v) and the factor indicators $\{Z_{M,A}(v)\}$ provide node-level factual evidence on how heterogeneous information affects predictive performance and structural properties.

Indicators & Pattern	ATE	SE	RR	PASS
$H_{\text{avg}}, D_{\text{min}} $ (11)	0.081	0.009	1.49	√
D_{\min} (1)	0.049	0.005	1.35	✓
H_{avg} (1)	0.037	0.017	1.22	\checkmark

Table 4: Factual evaluation of structural indicator patterns based on the average treatment effect (ATE), standard error (SE), and relative risk (RR). All three patterns satisfy the significance and robustness criteria (PASS, \checkmark), supporting the validity of the selected indicators as reliable metrics for quantifying structural causal effects under factual analysis.

4.3.3. Factual Analysis

Table 4 summarizes the factual causal-effect estimates for the three representative indicator patterns, evaluated using the Average Treatment Effect (ATE), standard error (SE), and relative risk (RR). To simplify notation, we denote the three patterns as

$$P_1: H^G(v) < H_{\text{avg}}^{\mathcal{G}}(v), \ D^G(v) < D_{\min}^{\mathcal{G}}(v);$$

$$P_2: D^G(v) < D_{\min}^{\mathcal{G}}(v);$$

$$P_3: H^G(v) < H_{\text{avg}}^{\mathcal{G}}(v).$$

$$(24)$$

Here, each inequality indicates that the corresponding factor on the homogeneous projection (G) is smaller than its aggregate counterpart on the heterogeneous graph (G). The factual evaluation focuses on the magnitude, stability, and reliability of causal effects under real observations, aiming to validate whether the selected structural indicators constitute meaningful metrics.

Pattern P₁—combining reductions in both homophily and local–global distribution discrepancy—shows the highest average treatment effect (ATE = 0.081) and a relative risk of 1.49, demonstrating the strongest and most stable causal influence among all patterns.

Pattern P_2 , defined solely by reduced distribution discrepancy, yields a moderate yet significant effect (ATE = 0.049, RR = 1.35), confirming that weakened local-global distinctiveness alone can substantially impact predictive outcomes.

Pattern P_3 , driven only by reduced homophily, exhibits a smaller but still significant effect (ATE = 0.037, RR = 1.22), indicating that homophily differences independently contribute to the factual performance gap between heterogeneous and homogeneous graphs.

All three patterns pass the factual significance and robustness checks (\checkmark in Table 4), supporting the validity of ATE, SE, and RR as reliable metrics for quantifying structural causal effects under factual analysis.

Indicators & Pattern	Mean Uplift	Median Uplift	PN	PS
$H_{\text{avg}}, D_{\text{min}} $ (11)	0.229	0.233	1.00	0.67
D_{\min} (1)	0.191	0.191	1.00	0.24
H_{avg} (1)	0.146	0.132	1.00	0.09

Table 5: Counterfactual evaluation of structural indicator patterns using simulated node-level outcomes. Mean Uplift represents the average counterfactual improvement in node prediction accuracy when the corresponding factor is present, and Median Uplift indicates the typical (50th-percentile) improvement across nodes. PN (probability of necessity) quantifies the proportion of nodes for which the factor is necessary to achieve correct prediction, while PS (probability of sufficiency) measures the proportion of nodes for which the factor alone is sufficient to produce correct prediction. All patterns show positive uplift values, confirming that each factor contributes positively under counterfactual evaluation.

4.3.4. Counterfactual Analysis

Table 5 reports the counterfactual evaluation results for the three structural indicator patterns defined in Equation 24. This analysis quantifies how

the removal of each factor would affect model performance by estimating four indicators: Mean Uplift, Median Uplift, PN, and PS. Mean and Median Uplift measure the average and typical reductions in node prediction accuracy when the corresponding factor is absent, reflecting the extent to which each factor prevents performance degradation. PN (probability of necessity) denotes the proportion of nodes that rely on a given factor to remain correctly predicted, whereas PS (probability of sufficiency) represents the proportion of nodes for which the factor alone is sufficient to sustain correct prediction once heterogeneity is removed.

All three patterns show positive uplift values, indicating that omitting any of the identified factors leads to observable declines in predictive accuracy. Pattern P_1 exhibits the highest uplift (mean = 0.229, median = 0.233) and the largest sufficiency proportion (PS = 0.67), demonstrating that the joint presence of low homophily and low distribution discrepancy most effectively preserves prediction accuracy under counterfactual removal. Pattern P_2 shows a moderate uplift (mean = 0.191) and a smaller PS (0.24), suggesting that distribution discrepancy alone remains an important but less dominant stabilizing factor. Pattern P_3 presents the smallest uplift (mean = 0.146) and limited sufficiency (PS = 0.09), indicating that homophily reduction also contributes positively but with weaker protective strength. Overall, the counterfactual results confirm that each structural factor plays a necessary and partially sufficient role in mitigating performance degradation when heterogeneous information is removed.

Indicators & Pattern	ATE (DR)	Consistency	E-value
$H_{\text{avg}}, D_{\text{min}} $ (11)	✓	5/5	2.35
D_{\min} (1)	\checkmark	5/5	2.04
H_{avg} (1)	\checkmark	5/5	1.74

Table 6: Validation through adjustment, consistency, and sensitivity analyses. Symbols indicate the evaluation outcome for the doubly robust estimation: \checkmark — ATE (DR) is consistent in direction and magnitude with the original ATE. The Consistency column shows the number of estimators with matching effect direction (out of five), and E-value quantifies the minimum strength of association that an unmeasured confounder would require with both the factor and the outcome to explain away the observed causal effect. All three patterns remain consistent and robust under sensitivity evaluation.

4.3.5. Minimal Sufficient Adjustment Set

To ensure that the causal effects identified in the previous analyses are not influenced by confounding, we introduce the minimal sufficient adjustment set (MSAS). A covariate set Z^* is minimal sufficient if it makes the treatment T independent of the potential outcomes (Y(1), Y(0)) and cannot be further reduced without reintroducing dependence:

$$(Y(1), Y(0)) \perp T \mid Z^*, \qquad \forall Z' \subsetneq Z^* : (Y(1), Y(0)) \not \perp {}^5T \mid Z'.$$
 (25)

In practice, Z^* is the smallest set of structural variables that must be controlled to remove confounding and make the causal effect identifiable. The average treatment effect (ATE) is then estimated under the MSAS using the doubly robust (DR) estimator:

$$\widehat{ATE}_{DR} = \frac{1}{n} \sum_{i=1}^{n} \left[\frac{T_i(Y_i - \hat{\mu}_1(Z_i))}{\hat{e}(Z_i)} - \frac{(1 - T_i)(Y_i - \hat{\mu}_0(Z_i))}{1 - \hat{e}(Z_i)} + \hat{\mu}_1(Z_i) - \hat{\mu}_0(Z_i) \right],$$
(26)

where $\hat{e}(Z_i) = P(T_i=1 \mid Z_i)$ is the estimated propensity score and $\hat{\mu}_t(Z_i) = \mathbb{E}[Y_i \mid T_i = t, Z_i]$ is the outcome model. If the estimated ATE remains similar in sign and magnitude to the unadjusted result, the identified structural factors are genuine causal contributors rather than correlated covariates.

As shown in Table 6, the ATEs estimated under the MSAS align with the factual and counterfactual results. When adjusting for each factor individually or jointly, the ATE (DR) values stay around 0.07 to 0.08, indicating that the causal effects of H and D are stable and not driven by correlated variables. Here, adjusting for H compares heterogeneous and homogeneous models at the same level of homophily, while adjusting for D controls differences in the local and global label distributions. The agreement across all adjustment settings supports that these structural factors directly contribute to the observed performance gains.

4.3.6. Cross-method Consistency

To further examine the robustness of the estimated causal effects, we perform a cross-method consistency check. For each of the three patterns P_1 , P_2 , and P_3 , effects are re-estimated using five complementary strategies: unadjusted difference-in-means, propensity score matching (PSM), inverse

 $^{^{5}\}bot$ denotes conditional independence.

probability weighting (IPW), doubly robust estimation (AIPW/DR), and targeted maximum likelihood estimation (TMLE).

The PSM estimator compares each treated sample with a matched control that has the closest estimated propensity score $\hat{e}(Z_i) = P(T_i=1 \mid Z_i)$:

$$\widehat{ATE}_{psm} = \frac{1}{n_1} \sum_{i:T_i=1} (Y_i - Y_{j(i)}), \qquad (27)$$

where n_1 is the number of treated samples, Y_i is the observed outcome of sample i, and j(i) denotes the index of its matched control with the nearest $\hat{e}(Z_i)$.

The TMLE estimator combines outcome regression and propensity modeling, updating the predictions $\hat{\mu}_t(Z_i) = \mathbb{E}[Y_i \mid T_i = t, Z_i]$ through a fluctuation step:

$$\widehat{ATE}_{tmle} = \frac{1}{n} \sum_{i=1}^{n} (\hat{\mu}_{1}^{*}(Z_{i}) - \hat{\mu}_{0}^{*}(Z_{i})),$$
 (28)

where $\hat{\mu}_t^*(Z_i)$ is the updated prediction after the TMLE adjustment and n is the total sample size.

Agreement in effect direction and magnitude across all methods, together with overlapping confidence intervals, is regarded as evidence of cross-method consistency. When the estimated effects remain positive and comparable across all estimation strategies, it indicates that the causal conclusions are robust to modeling assumptions and estimator choices.

4.3.7. Sensitivity Analysis

To further evaluate the robustness of the estimated causal effects against potential unmeasured confounding, we perform a sensitivity analysis using the E-value. The E-value quantifies the minimum strength of association that an unmeasured confounder would need to have with both the factor (pattern) and the outcome to fully explain away the observed effect. Formally, for an estimated risk ratio RR, the E-value is defined as

E-value =
$$RR + \sqrt{RR \times (RR - 1)}$$
. (29)

A larger E-value indicates greater robustness, as stronger confounding would be required to nullify the estimated causal relationship.

As summarized in Table 6, all three patterns P_1 , P_2 , and P_3 maintain full estimator consistency (5/5) and yield E-values above 1.7. P_1 (2.35) demonstrates the highest robustness, indicating that only a strong unmeasured

confounder could eliminate its effect. P_2 (2.04) remains stable, suggesting that distribution discrepancy alone provides a reliable causal contribution. P_3 (1.74) shows moderate robustness, implying that the homophily factor is comparatively more sensitive to potential confounding. Overall, all three patterns meet the robustness criteria and remain valid under sensitivity evaluation.

4.3.8. Structural Pattern Distribution

To further understand how heterogeneous information influences structural properties, we examine the occurrence of the three identified patterns P_1 , P_2 , and P_3 across all HGNN datasets. For each dataset, we compute the proportion of nodes that satisfy each structural pattern and then take the average across datasets. The results are summarized in Table 7.

Pattern	Definition	Average occurrence (%)
P_1	$H^G < H_{\text{avg}}^{\mathcal{G}}, \ D^G < D_{\min}^{\mathcal{G}}$	57.67
P_2	$D^G < D_{\min}^{\mathcal{G}}$	76.05
P_3	$H^G < H_{ ext{avg}}^{\mathcal{G}}$	59.47
None	No pattern satisfied	22.15

Table 7: Average occurrence of structural patterns across all HGNN datasets.

The results show that the patterns P₁, P₂, and P₃ occur frequently across heterogeneous graphs, with average probabilities of 57.67%, 76.05%, and 59.47%, respectively. This indicates that introducing heterogeneous information consistently increases both homophily and local-to-global distribution discrepancy for a large portion of nodes. Only 22.15% of nodes do not exhibit any of these patterns, suggesting that heterogeneity primarily enhances structural distinctiveness rather than diluting it. These findings provide direct empirical evidence for the causal pathway from heterogeneous information to structural signal strengthening, which ultimately improves node-level separability and classification accuracy.

5. Conclusion

To address the lack of rigorous evidence on the effectiveness of HGNNs for node classification, we conduct a comprehensive causal analysis that separates model architecture from heterogeneous information. The results show

that model architecture and complexity have no causal effect on node classification performance. In contrast, heterogeneous information exerts a positive causal effect by reshaping graph structure, increasing homophily, and enlarging the difference between local and global label distributions, which makes node classes more distinguishable and improves predictive accuracy.

References

- [1] Z. Wu, S. Pan, F. Chen, G. Long, C. Zhang, S. Y. Philip, A comprehensive survey on graph neural networks, IEEE transactions on neural networks and learning systems 32 (1) (2020) 4–24.
- [2] F. Xia, K. Sun, S. Yu, A. Aziz, L. Wan, S. Pan, H. Liu, Graph learning: A survey, IEEE Transactions on Artificial Intelligence 2 (2) (2021) 109– 127.
- [3] Y. Bei, W. Chen, H. Chen, S. Zhou, C. Yang, J. Fan, L. Huang, J. Bu, Correlation-aware graph convolutional networks for multi-label node classification, in: Proceedings of the 31st ACM SIGKDD Conference on Knowledge Discovery and Data Mining V. 1, 2025, pp. 37–48.
- [4] X. Li, J. Saúde, Explain graph neural networks to understand weighted graph features in node classification, in: International Cross-Domain Conference for Machine Learning and Knowledge Extraction, Springer, 2020, pp. 57–76.
- [5] S. Gong, J. Ni, N. Sachdeva, C. Yang, W. Jin, Gc4nc: A benchmark framework for graph condensation on node classification with new insights, arXiv preprint arXiv:2406.16715 (2024).
- [6] X. Zhao, H. Chen, Z. Xing, C. Miao, Brain-inspired search engine assistant based on knowledge graph, IEEE Transactions on Neural Networks and Learning Systems 34 (8) (2021) 4386–4400.
- [7] A. Ali, J. Li, H. Chen, A. B. A. Ajlouni, A binary classification social network dataset for graph machine learning, arXiv preprint arXiv:2503.02397 (2025).

- [8] Z.-X. Ma, Z.-D. Chen, L.-J. Zhao, Z.-C. Zhang, X. Luo, X.-S. Xu, Crosslayer and cross-sample feature optimization network for few-shot fine-grained image classification, in: Proceedings of the AAAI conference on artificial intelligence, Vol. 38, 2024, pp. 4136–4144.
- [9] K. Sharma, Y.-C. Lee, S. Nambi, A. Salian, S. Shah, S.-W. Kim, S. Kumar, A survey of graph neural networks for social recommender systems, ACM Computing Surveys 56 (10) (2024) 1–34.
- [10] H. Li, S. Li, J. Sun, Z. Xing, X. Peng, M. Liu, X. Zhao, Improving api caveats accessibility by mining api caveats knowledge graph, in: 2018 IEEE International Conference on Software Maintenance and Evolution (ICSME), IEEE, 2018, pp. 183–193.
- [11] X. Yang, X. Zhao, Z. Shen, A generalizable anomaly detection method in dynamic graphs, in: Proceedings of the AAAI Conference on Artificial Intelligence, Vol. 39, 2025, pp. 22001–22009.
- [12] H. Du, L. Yuan, Q. Yang, X. Chen, Y. Zhao, H. Ji, F. Zhuang, C. Yang, G. Kou, Identifying evidence subgraphs for financial risk detection via graph counterfactual and factual reasoning, arXiv preprint arXiv:2503.06441 (2025).
- [13] X. Zhao, S. Liu, S.-Y. Yang, C. Miao, Medrag: Enhancing retrieval-augmented generation with knowledge graph-elicited reasoning for healthcare copilot, in: Proceedings of the ACM on Web Conference 2025, 2025, pp. 4442–4457.
- [14] X. Zhao, S. Liu, S.-Y. Yang, C. Miao, A smart multimodal healthcare copilot with powerful llm reasoning, arXiv preprint arXiv:2506.02470 (2025).
- [15] X. Li, N. C. Dvornek, Y. Zhou, J. Zhuang, P. Ventola, J. S. Duncan, Graph neural network for interpreting task-fmri biomarkers, in: International conference on medical image computing and computer-assisted intervention, Springer, 2019, pp. 485–493.
- [16] J. Qiao, W. Gao, J. Jin, D. Wang, X. Guo, B. Manavalan, L. Wei, Molecular pretraining models towards molecular property prediction, Science China Information Sciences 68 (7) (2025) 170104.

- [17] J. Qiao, J. Jin, D. Wang, S. Teng, J. Zhang, X. Yang, Y. Liu, Y. Wang, L. Cui, Q. Zou, et al., A self-conformation-aware pre-training framework for molecular property prediction with substructure interpretability, Nature Communications 16 (1) (2025) 4382.
- [18] P. Velickovic, G. Cucurull, A. Casanova, A. Romero, P. Lio, Y. Bengio, et al., Graph attention networks, stat 1050 (20) (2017) 10–48550.
- [19] W. Hamilton, Z. Ying, J. Leskovec, Inductive representation learning on large graphs, Advances in neural information processing systems 30 (2017).
- [20] X. Zhao, Explainable q&a system based on domain-specific knowledge graph (2021).
- [21] J. Gilmer, S. S. Schoenholz, P. F. Riley, O. Vinyals, G. E. Dahl, Neural message passing for quantum chemistry, in: International conference on machine learning, PMLR, 2017, pp. 1263–1272.
- [22] X. Yang, X. Zhao, Z. Shen, A unified gradient regularization method for heterogeneous graph neural networks, Neural Networks (2025) 108104.
- [23] C. Shi, Y. Li, J. Zhang, Y. Sun, S. Y. Philip, A survey of heterogeneous information network analysis, IEEE Transactions on Knowledge and Data Engineering 29 (1) (2016) 17–37.
- [24] C. Yang, Y. Xiao, Y. Zhang, Y. Sun, J. Han, Heterogeneous network representation learning: A unified framework with survey and benchmark, IEEE Transactions on Knowledge and Data Engineering 34 (10) (2020) 4854–4873.
- [25] C. Zhang, D. Song, C. Huang, A. Swami, N. V. Chawla, Heterogeneous graph neural network, in: Proceedings of the 25th ACM SIGKDD international conference on knowledge discovery & data mining, 2019, pp. 793–803.
- [26] X. Wang, D. Bo, C. Shi, S. Fan, Y. Ye, S. Y. Philip, A survey on heterogeneous graph embedding: methods, techniques, applications and sources, IEEE Transactions on Big Data 9 (2) (2022) 415–436.

- [27] Y. Yang, J. Chen, X. Gao, Y. Xiang, Dual de-confounded causal intervention method for knowledge graph error detection, Knowledge-Based Systems 305 (2024) 112644.
- [28] T. Ban, L. Chen, D. Lyu, X. Wang, Q. Zhu, H. Chen, Llm-driven causal discovery via harmonized prior, IEEE Transactions on Knowledge and Data Engineering (2025).
- [29] Y. Chen, J. Cao, Y. Wang, J. Wu, H. Chen, G. Xu, Causal variational inference for deconfounded multi-behavior recommendation, ACM Transactions on Information Systems (2025).
- [30] J. Zhu, X. Wu, M. Usman, X. Wang, H. Chen, Link prediction in continuous-time dynamic heterogeneous graphs with causality of event types, International Journal of Crowd Science 6 (2) (2022) 80–91.
- [31] B. Jing, D. Zhou, K. Ren, C. Yang, Causality-aware spatiotemporal graph neural networks for spatiotemporal time series imputation, in: Proceedings of the 33rd ACM International Conference on Information and Knowledge Management, 2024, pp. 1027–1037.
- [32] S. Adhikari, E. Zheleva, Inferring individual direct causal effects under heterogeneous peer influence, Machine Learning 114 (4) (2025) 113.
- [33] Z. Zhao, Y. Bai, R. Xiong, Q. Cao, C. Ma, N. Jiang, F. Wu, K. Kuang, Learning individual treatment effects under heterogeneous interference in networks, ACM Transactions on Knowledge Discovery from Data 18 (8) (2024) 1–21.
- [34] Y. Wu, Y. Yuan, Estimating heterogeneous causal effect on networks via orthogonal learning, arXiv preprint arXiv:2509.18484 (2025).
- [35] Q. Lv, M. Ding, Q. Liu, Y. Chen, W. Feng, S. He, C. Zhou, J. Jiang, Y. Dong, J. Tang, Are we really making much progress? revisiting, benchmarking and refining heterogeneous graph neural networks, in: Proceedings of the 27th ACM SIGKDD conference on knowledge discovery & data mining, 2021, pp. 1150–1160.
- [36] M. Schlichtkrull, T. N. Kipf, P. Bloem, R. Van Den Berg, I. Titov, M. Welling, Modeling relational data with graph convolutional networks,

- in: The semantic web: 15th international conference, ESWC 2018, Heraklion, Crete, Greece, June 3–7, 2018, proceedings 15, Springer, 2018, pp. 593–607.
- [37] Y. Ma, X. Liu, N. Shah, J. Tang, Is homophily a necessity for graph neural networks?, arXiv preprint arXiv:2106.06134 (2021).
- [38] J. Zhu, Y. Yan, L. Zhao, M. Heimann, L. Akoglu, D. Koutra, Beyond homophily in graph neural networks: Current limitations and effective designs, Advances in neural information processing systems 33 (2020) 7793–7804.
- [39] S. Luan, C. Hua, M. Xu, Q. Lu, J. Zhu, X.-W. Chang, J. Fu, J. Leskovec, D. Precup, When do graph neural networks help with node classification? investigating the homophily principle on node distinguishability, Advances in Neural Information Processing Systems 36 (2024).
- [40] J. Zhu, G. Li, Y.-A. Yang, J. Zhu, X. Cui, D. Koutra, On the impact of feature heterophily on link prediction with graph neural networks, Advances in Neural Information Processing Systems 37 (2024) 65823– 65851.
- [41] Z. Liu, Y. Fang, C. Liu, S. C. Hoi, Node-wise localization of graph neural networks, arXiv preprint arXiv:2110.14322 (2021).
- [42] G. Yehudai, E. Fetaya, E. Meirom, G. Chechik, H. Maron, From local structures to size generalization in graph neural networks, in: International Conference on Machine Learning, PMLR, 2021, pp. 11975–11986.
- [43] D. Loveland, J. Zhu, M. Heimann, B. Fish, M. T. Schaub, D. Koutra, On performance discrepancies across local homophily levels in graph neural networks, in: Learning on Graphs Conference, PMLR, 2024, pp. 6–1.
- [44] Z. Hu, Y. Dong, K. Wang, Y. Sun, Heterogeneous graph transformer, in: Proceedings of the web conference 2020, 2020, pp. 2704–2710.
- [45] X. Wang, H. Ji, C. Shi, B. Wang, Y. Ye, P. Cui, P. S. Yu, Heterogeneous graph attention network, in: The world wide web conference, 2019, pp. 2022–2032.

- [46] X. Fu, J. Zhang, Z. Meng, I. King, Magnn: Metapath aggregated graph neural network for heterogeneous graph embedding, in: Proceedings of the web conference 2020, 2020, pp. 2331–2341.
- [47] S. Yun, M. Jeong, R. Kim, J. Kang, H. J. Kim, Graph transformer networks, Advances in neural information processing systems 32 (2019).
- [48] J. Zhao, X. Wang, C. Shi, Z. Liu, Y. Ye, Network schema preserving heterogeneous information network embedding, in: International joint conference on artificial intelligence (IJCAI), 2020.
- [49] Q. Mao, Z. Liu, C. Liu, J. Sun, Hinormer: Representation learning on heterogeneous information networks with graph transformer, in: Proceedings of the ACM Web Conference 2023, 2023, pp. 599–610.
- [50] X. Yang, M. Yan, S. Pan, X. Ye, D. Fan, Simple and efficient heterogeneous graph neural network, in: Proceedings of the AAAI conference on artificial intelligence, Vol. 37, 2023, pp. 10816–10824.
- [51] D. B. Rubin, Estimating causal effects of treatments in randomized and nonrandomized studies., Journal of educational Psychology 66 (5) (1974) 688.
- [52] J. Sekhon, The neyman—rubin model of causal inference and estimation via matching methods (2008).
- [53] L. Cotta, B. Bevilacqua, N. Ahmed, B. Ribeiro, Causal lifting and link prediction, Proceedings of the Royal Society A 479 (2276) (2023) 20230121.
- [54] G. Chen, Y. Wang, F. Guo, Q. Guo, J. Shao, H. Shen, X. Cheng, Causality and independence enhancement for biased node classification, in: Proceedings of the 32nd ACM international conference on information and knowledge management, 2023, pp. 203–212.
- [55] J. Sun, Y. Sheng, L. He, Y. Qin, M. Liu, T. Jia, Cegrl-tkgr: A causal enhanced graph representation learning framework for temporal knowledge graph reasoning, arXiv preprint arXiv:2408.07911 (2024).

- [56] S. Jiang, Y. Sun, Estimating causal effects on networked observational data via representation learning, in: Proceedings of the 31st ACM International Conference on Information & Knowledge Management, 2022, pp. 852–861.
- [57] X. Du, J. Li, D. Cheng, L. Liu, W. Gao, X. Chen, Estimating peer direct and indirect effects in observational network data, arXiv preprint arXiv:2408.11492 (2024).
- [58] A. Farzam, A. R. Tannenbaum, G. Sapiro, From geometry to causality-ricci curvature and the reliability of causal inference on networks, in: Forty-first International Conference on Machine Learning, ICML 2024, Vienna, Austria, July 21-27, 2024, OpenReview.net, 2024. URL https://openreview.net/forum?id=4DAl3IsvlU
- [59] R. Cai, Z. Yang, W. Chen, Y. Yan, Z. Hao, Generalization bound for estimating causal effects from observational network data, in: Proceedings of the 32nd ACM International Conference on Information and Knowledge Management, 2023, pp. 163–172.
- [60] B. Hu, Z. An, Z. Wu, K. Tu, Z. Liu, Z. Zhang, J. Zhou, Y. Feng, J. Chen, Graph disentangle causal model: Enhancing causal inference in networked observational data, in: Proceedings of the Eighteenth ACM International Conference on Web Search and Data Mining, 2025, pp. 1–9.
- [61] Y. Sui, C. Tang, Z. Chu, J. Fang, Y. Gao, Q. Cui, L. Li, J. Zhou, X. Wang, Invariant graph learning for causal effect estimation, in: Proceedings of the ACM Web Conference 2024, 2024, pp. 2552–2562.
- [62] X. Wang, T. Ban, L. Chen, D. Lyu, Q. Zhu, H. Chen, Large-scale hierarchical causal discovery via weak prior knowledge, IEEE Transactions on Knowledge and Data Engineering (2025).
- [63] T. Ban, X. Wang, L. Chen, D. Lyu, X. Fan, H. Chen, Harnessing the power of knowledge graphs to improve causal discovery, IEEE Transactions on Emerging Topics in Computational Intelligence (2025).
- [64] M. B. Begum, A. Yogeshwaran, N. Nagarajan, P. Rajalakshmi, Dynamic network security leveraging efficient covinet with granger causality-

- inspired graph neural networks for data compression in cloud iot devices, Knowledge-Based Systems 309 (2025) 112859.
- [65] H. Gao, P. Qiao, Y. Jin, F. Wu, J. Li, C. Zheng, Introducing diminutive causal structure into graph representation learning, Knowledge-Based Systems 293 (2024) 111592.
- [66] A. Khaled, A. M. T. Elsir, P. Wang, Y. Shen, Q. Zhang, A graph-based approach for traffic prediction using similarity and causal relations between nodes, Knowledge-Based Systems 296 (2024) 111913.
- [67] W. G. Cochran, The $\chi 2$ test of goodness of fit, The Annals of mathematical statistics (1952) 315–345.
- [68] A. Agresti, M. Kateri, Categorical data analysis, in: International encyclopedia of statistical science, Springer, 2025, pp. 408–411.
- [69] Y. Benjamini, Y. Hochberg, Controlling the false discovery rate: a practical and powerful approach to multiple testing, Journal of the Royal statistical society: series B (Methodological) 57 (1) (1995) 289–300.
- [70] R. Jaeschke, J. Singer, G. H. Guyatt, Measurement of health status: ascertaining the minimal clinically important difference, Controlled clinical trials 10 (4) (1989) 407–415.
- [71] H. Han, T. Zhao, C. Yang, H. Zhang, Y. Liu, X. Wang, C. Shi, Openhgnn: an open source toolkit for heterogeneous graph neural network, in: Proceedings of the 31st ACM International Conference on Information & Knowledge Management, 2022, pp. 3993–3997.
- [72] T. N. Kipf, M. Welling, Semi-supervised classification with graph convolutional networks, arXiv preprint arXiv:1609.02907 (2016).
- [73] Y. Luo, L. Shi, X.-M. Wu, Classic gnns are strong baselines: Reassessing gnns for node classification, arXiv preprint arXiv:2406.08993 (2024).
- [74] S. Zhu, C. Zhou, S. Pan, X. Zhu, B. Wang, Relation structure-aware heterogeneous graph neural network, in: 2019 IEEE international conference on data mining (ICDM), IEEE, 2019, pp. 1534–1539.

- [75] P. Yu, C. Fu, Y. Yu, C. Huang, Z. Zhao, J. Dong, Multiplex heterogeneous graph convolutional network, in: Proceedings of the 28th ACM SIGKDD Conference on Knowledge Discovery and Data Mining, 2022, pp. 2377–2387.
- [76] Z. Zhou, J. Shi, R. Yang, Y. Zou, Q. Li, Slotgat: slot-based message passing for heterogeneous graphs, in: International Conference on Machine Learning, PMLR, 2023, pp. 42644–42657.
- [77] J. Hu, B. Hooi, B. He, Efficient heterogeneous graph learning via random projection, IEEE Transactions on Knowledge and Data Engineering (2024).
- [78] Y. Mo, F. Nie, P. Hu, H. T. Shen, Z. Zhang, X. Wang, X. Zhu, Self-supervised heterogeneous graph learning: a homophily and heterogeneity view, in: The Twelfth International Conference on Learning Representations.
- [79] X. Zhao, Y. Liu, Y. Xu, Y. Yang, X. Luo, C. Miao, Heterogeneous star graph attention network for product attributes prediction, Advanced Engineering Informatics 51 (2022) 101447.
- [80] H. Hong, H. Guo, Y. Lin, X. Yang, Z. Li, J. Ye, An attention-based graph neural network for heterogeneous structural learning, in: Proceedings of the AAAI conference on artificial intelligence, Vol. 34, 2020, pp. 4132–4139.
- [81] X. Wang, N. Liu, H. Han, C. Shi, Self-supervised heterogeneous graph neural network with co-contrastive learning, in: Proceedings of the 27th ACM SIGKDD conference on knowledge discovery & data mining, 2021, pp. 1726–1736.
- [82] X. Li, D. Ding, B. Kao, Y. Sun, N. Mamoulis, Leveraging meta-path contexts for classification in heterogeneous information networks, in: 2021 IEEE 37th International Conference on Data Engineering (ICDE), IEEE, 2021, pp. 912–923.
- [83] J. Zhao, X. Wang, C. Shi, B. Hu, G. Song, Y. Ye, Heterogeneous graph structure learning for graph neural networks, in: Proceedings of the AAAI conference on artificial intelligence, Vol. 35, 2021, pp. 4697–4705.

- [84] J. Guo, L. Du, W. Bi, Q. Fu, X. Ma, X. Chen, S. Han, D. Zhang, Y. Zhang, Homophily-oriented heterogeneous graph rewiring, in: Proceedings of the ACM Web Conference 2023, 2023, pp. 511–522.
- [85] X. Fu, I. King, Mecch: metapath context convolution-based heterogeneous graph neural networks, Neural Networks 170 (2024) 266–275.
- [86] Z. Lu, Y. Fang, C. Yang, C. Shi, Heterogeneous graph transformer with poly-tokenization, International Joint Conferences on Artificial Intelligence, 2024.
- [87] C. Li, J. Fu, Y. Yan, Z. Zhao, Q. Zeng, Higher order heterogeneous graph neural network based on node attribute enhancement, Expert Systems with Applications 238 (2024) 122404.
- [88] C. Park, D. Kim, J. Han, H. Yu, Unsupervised attributed multiplex network embedding, in: Proceedings of the AAAI conference on artificial intelligence, Vol. 34, 2020, pp. 5371–5378.
- [89] H. Pei, B. Wei, K. C.-C. Chang, Y. Lei, B. Yang, Geom-gcn: Geometric graph convolutional networks, arXiv preprint arXiv:2002.05287 (2020).